Challenges of High-resolution Diffusion Imaging of the Human Medial Temporal Lobe in Alzheimer Disease

Michael M. Zeineh, MD, PhD, Samantha Holdsworth, PhD,* Stefan Skare, PhD,† Scott W. Atlas, MD,* and Roland Bammer, PhD**

Abstract: The human medial temporal lobe performs an essential role in memory formation and retrieval. Diseases involving the hippocampus such as Alzheimer disease present a unique opportunity for advanced imaging techniques to detect abnormalities at an early stage. In particular, it is possible that diffusion imaging will measure abnormal microarchitecture beyond the realm of macroscopic imaging. However, this task is formidable because of the detailed anatomy of the medial temporal lobe, the difficulties in obtaining high-quality diffusion images of adequate resolution, and the challenges in diffusion data processing. Moreover, it is unclear if any differences will be significant for an individual patient or simply groups of patients. Successful endeavors will need to address each of these challenges in an integrated fashion. The rewards of such analysis may be detection of microscopic disease in vivo, which could represent a landmark accomplishment for the field of neuroradiology.

Key Words: diffusion, tractography, hippocampus, Alzheimer, medial temporal lobe, anisotropy

(*Top Magn Reson Imaging* 2010;21: 355–365)

The overall aim of this article was to discuss the application of diffusion tensor imaging (DTI) to the medial temporal lobe (MTL), with particular attention to interrogating abnormalities in Alzheimer disease (AD). We provide in-depth description of the underlying neuroanatomy and relevant neuropathology in AD, and we review some of the impressive clinical DTI studies done to date. After a detailed discussion on the limitations and challenges of current implementations of DTI, we provide some recommendations for improving the image quality and reproducibility for future scientific studies as well as clinical applications. The same techniques and concepts described here also apply to diseases such as mesial temporal sclerosis and other degenerative disorders of the temporal lobe.

A BRIEF HISTORY OF STUDIES OF MEDIAL TEMPORAL LOBE FUNCTION

An Italian anatomist named Julius Caesar Arantius was the first to name and describe the hippocampus in 1587.[1,2] The term translates as "horse-caterpillar." Although in Greek and Roman mythology, *hippocampus* refers to a marine god sitting atop a seahorse, it is believed Arantius meant the small sea creature. He also applied the name *bombycinus vermis*, Latin for silkworm, although this was not his preferred name for the structure. A complicated history of MTL terminology ensued. The term *hippocampus* still stands, but several other terms have been adopted such as *pez hippocampi* and *Ammon's horn*, which now have specific references to microanatomy although not necessarily consistent with their historical derivation.

For some time, the hippocampus was thought to be primarily important for olfactory processing. In a 1937 article, Papez (pronounced *pāpes*) tabulated some of the known clinical conditions affecting the hippocampus, cingulum, mammillary bodies, and anterior thalamus. For example, he noted that rabies was known to affect the hippocampus and result in "emotional perturbation."[3] He theorized that these structures were critical for emotional processing, and together, they have become known as the circuit of Papez. It was not until the 1950s with studies of patient Henry Gustav Molaison, known while he was alive as H.M., that the nature of hippocampal function became known. H.M. underwent bilateral medial temporal lobectomy for epilepsy and subsequently developed profound and permanent anterograde amnesia.[4,5] In the past 40 years, extensive work has been conducted studying the neural substrate of memory, focusing on the hippocampus and surrounding structures, collectively termed the *medial temporal lobe*. These inquiries have used a spectrum of investigative techniques including electrophysiology, animal and human lesion studies, molecular biology, neurochemistry, neural modeling, and various forms of brain imaging in humans and animals—all with the goal of elucidating how the MTL functions intrinsically and interacts with the rest of the brain to carry out mnemonic function. A central theme uniting all of these studies is that memory formation requires neuronal networks developing and strengthening their interconnections to form associations.[6] The hippocampus, the centerpiece of the MTL, is the most important component of the networks underlying learning and long-term consolidation of information.

NEUROANATOMY: HIPPOCAMPAL SUBFIELDS AND CONNECTIVITY

From an imaging perspective, the MTL is a unique part of the brain for many reasons. First, the complexities of its anatomy are readily apparent on modern MR structural imaging. Second, these complexities are largely consistent across subjects, barring differences in brain size and relatively minor differences in hippocampal development. Finally, the hippocampus has the distinction that its only known role is memory formation, which is crucial to normal cognitive function. This is in contradistinction to structures such as 1) the cerebellar hemispheres, which have intricate structure relatively consistent across subjects but are not essential to cognition; 2) the thalamus, which is important to cognition and the sensorium, in which intricate structure is not apparent on conventional imaging, although its appearance is consistent across subjects; and 3) the neocortex, which is essential for language and memory among other eloquent functions but has relatively homogeneous gross structure that varies significantly across subjects. Hence, a detailed understanding

From the *Stanford University, Stanford, CA; and †Karolinska Institutet, Stockholm, Sweden.
Reprints: Michael Maroun Zeineh, MD, PhD, Stanford University, Room S-047, 300 Pasteur Dr, Stanford, CA 94305-5105 (e-mail: mzeineh@stanford.edu).
This study was supported by the RSNA Research and Education Foundation Research Fellow Award and by General Electric.
Disclosure: The authors declare no conflict of interest.

of hippocampal gross and microanatomy is beneficial for a discussion of connectivity. In addition, alterations in anatomy and connectivity may be easier to discern from intersubject variance because of the relatively consistent anatomy.

The MTL is a compact structure with several components (Fig. 1). It can be roughly divided into two parts: the hippocampus proper and the adjacent neocortical areas. The nearby cortical areas project to the hippocampus proper, and the hippocampus proper has an internal system of projections that send output back to the nearby cortical areas.[8,9] The details of connectivity are derived from tracer studies on the macaque monkey, whose brain has a direct anatomical correspondence with the human brain.[10]

The entorhinal cortex (ERC), which lies in the anterior portion of the parahippocampal gyrus and borders the anterior hippocampus, is the main gateway of input to and output from the hippocampus proper.[11] It receives most of its projections from two adjacent areas: the perirhinal cortex (PRC) and the parahippocampal cortex (PHC). Besides the perirhinal and parahippocampal contributions, the ERC receives input from polymodal cingulate/retrosplenial cortex, dorsal superior temporal sulcus, orbitofrontal cortex, the olfactory bulb, and parainsular cortex. Both the PRC and PHC receive widespread projections from many cerebral areas.

The essential circuit diagram of the hippocampus proper is a loop (Fig. 2). The main circuit starts with cells in layers II and VI of the ERC projecting via a white matter tract called the *angular bundle* to innervate primarily the dentate gyrus and CA 3 (cornu ammonis 3).[12] This comprises the perforant path, labeled as such because fibers perforate the subiculum on the way to the dentate gyrus. From the dentate gyrus, neurons synapse successively to fields CA 3, CA 1, the subiculum, and back to layer V of the ERC, where output returns to the PHC and PRC. A complementary projection from entorhinal layers III and V targets primarily the distal half of this circuitry loop, namely CA 1 and the subiculum.

Extensive interconnections are present within the dentate and CA 3 fields. The hippocampus also interacts with subcortical structures: an output detour is taken from CA 3, the subiculum, and ERC, via the fornix, a white matter tract that attaches to the inferior border of the septum pellucidum and synapses with the mammillary nuclei within the hypothalamus as well as the septal nuclei.

These are the most basic of pathways, and there are numerous other connections at each stage that are beyond the scope of this article. A limitation in this model is that it is almost entirely derived from animal work, with only minimal tracing studies done on human specimens, which suggested the alvear pathway may be more important in humans than in monkeys.[13,14]

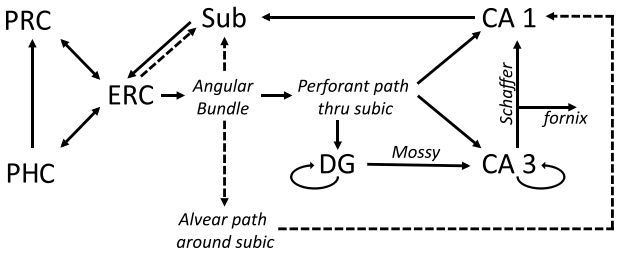

FIGURE 2. Pathways of the MTL. Solid lines indicate major pathways, and dotted lines are minor pathways. CA 1 indicates cornu ammonis 1; CA 2, 3, CA fields 2 and 3; CoS, collateral sulcus; DG, dentate gyrus; FG, fusiform gyrus; Sub, subiculum. ERC indicates entorhinal cortex; PHC, parahippocampal cortex; PRC, Perirhinal Cortex.

It is particularly important to note the scale of the images in Figure 1. The entirety of the hippocampus and adjacent substructures lies within a span of approximately 2 to 2.5 cm superoinferiorly, the height of the hippocampus proper including the subiculum is only approximately 6 to 8 mm, and the height of CA 1 is only approximately 1.5 mm.

AD AND THE MEDIAL TEMPORAL LOBE

Intensive investigations have sought to define the relationship between hippocampal dysfunction and AD, in which impaired memory formation is a distinguishing feature. Beginning in the MTL, a complex and incompletely understood interplay of intracellular neurofibrillary tangles and extracellular amyloid plaques likely contributes to synaptic and neural degeneration.[15–19] By the time a clinical diagnosis is possible, there has been extensive neuronal destruction,[19] and not surprisingly, there is no effective treatment for the disease. Because any effective prevention or treatment will need to occur before this neuronal loss, there is a great need for preclinical diagnosis of patients who will develop AD. Some of the well-studied methods attempting preclinical detection include structural magnetic resonance imaging (MRI),[20,21] functional MRI,[22,23] resting-state functional MRI,[24] diffusion tensor MRI (DTI),[25] cerebral spinal fluid (CSF)

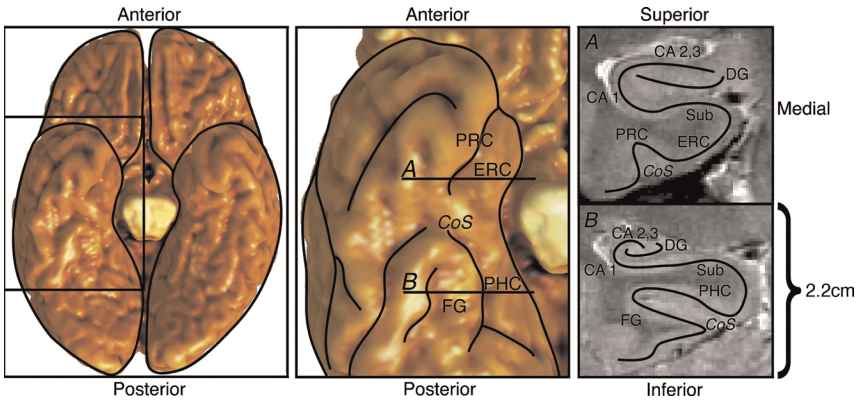

FIGURE 1. Anatomical diagram, with an inferior view of the temporal lobe at the left, and coronal sections from the 2 indicated slices at the right. A, Anterior slice through ERC. B, Posterior slice through parahippocampal cortex. CA 1 indicates cornu ammonis 1; CA 2, 3, CA fields 2 and 3; CoS, collateral sulcus; DG, dentate gyrus; FG, fusiform gyrus; Sub, subiculum. Reproduced from Zeineh et al,[7] adding a scale bar. ERC indicates entorhinal cortex; PHC, parahippocampal cortex; PRC, Perirhinal Cortex. Figure 1 can be viewed online in color at www.topicsinmri.com.

biomarkers,[26] and fluoro-deoxy glucose-positron emission tomography.[23] However, all of these are indirect measures of AD pathology and are typically significant at the group level, often with limited specificity and sensitivity. There remains a need for more accurate noninvasive preclinical imaging. More recent developments include the tracer Pittsburgh compound B (PIB), a PET tracer that binds amyloid.[27] Unfortunately, PIB is not specific to the subtype of amyloid, and in addition to amyloid plaques associated with AD, PIB is positive for amyloid angiopathy, which is common in the elderly and not strongly associated with AD.[28]

Given the current theory that long-term memory requires neural connectivity centered in the MTL, and given that memory formation is impaired in AD, measurements of connectivity may quantitatively ascertain mnemonic capability and the relevant impairment in diseases of the MTL such as AD. Neuropathological data suggest that cell loss in the ERC is marked in AD, particularly at early stages, concordant with neurofibrillary tangle pathology, which is known to start in the ERC.[29–31] Thus, DTI is uniquely poised to measure the neuronal loss in the MTL. Tractography is a form of diffusion tensor processing that attempts to identify tracts corresponding to white matter fascicles, and it may demonstrate some promise for AD.

This article will explore the challenges involved in using DTI of the MTL, with suggestions for more consistent and sensitive research and clinical studies. This is of interest in the field of neuroradiology where there are no specific findings of AD, especially at an early stage.

ROLE OF DTI IN AD

The axonal destruction associated with neurofibrillary (ie, plaque and tangle) pathology may be measurable by DTI. Diffusion-weighted imaging is sensitive to both the direction and theh magnitude of proton diffusion. In white matter, diffusion progresses primarily along the path of the axon, resulting in anisotropy in the pattern of diffusion. This is typically quantified as the fractional anisotropy (FA), a measure of how strong the diffusion is along the leading diffusion direction. The main contribution to this anisotropy is the orientation of the axons within the volume of a pixel.[32] Hence, axonal degeneration secondary to neurofibrillary-driven neural degeneration should be evident in quantitative diffusion-weighted imaging.

Many of the landmark diffusion studies in the literature demonstrate that some portion of the MTL exhibits abnormal diffusion characteristics in AD and/or MCI patients compared to healthy controls.[33–43] Similar but more minor changes are noted in mild cognitive impairment, a preclinical state that progresses to AD at a rate of approximately 10% to 15% a year. Two literature reviews and one meta-analysis more exhaustively summarize the results.[34,44,45] However, these alterations are minor among larger study groups and would not translate into useful thresholds on the single-subject level.

A detailed examination of the applied method finds significant variation in acquisition, processing, and in the exact location and type of result, summarized in Table 1. Perhaps one of the biggest contributors to the inconsistencies in these studies is the technical hurdles associated with the diffusion image acquisition and processing. Many of the challenges associated with performing DTI and subsequent tractography is described in detail below.

SUMMARY OF DTI STUDIES OF THE MTL IN AD

Acquisition Challenges

Teasing apart at least some of the microstructure of the MTL, such as the perforant pathway, requires high-resolution diffusion-tensor imaging. However, even typical DTI is fraught with both acquisition and processing challenges under common circumstances,[51,52] and many of these problems are exacerbated in the MTL.

A number of methods that can be used to acquire the DTI data; echo-planar imaging (EPI) is typically used for its speed and relative insensitivity to motion. However, EPI is subject to numerous types of artifact including susceptibility distortions and signal loss. These distortions typically occur where the magnetic field is inhomogeneous, such as at air-tissue interfaces. With regard to the MTL, the petrous apices, which are often pneumatized, can be a markedly significant source of this artifact. For EPI in any orientation, it is useful to perform parallel imaging along the phase-encode direction because the slow bandwidth along this direction causes severe image distortion. Parallel imaging techniques, such as sensitivity encoding or generalized autocalibrating partial parallel acquisition (GRAPPA) is known to significantly reduce distortions near the MTL. However, only 3 studies of the MTL in AD reviewed here have used parallel imaging (Table 1).

Typical structural imaging of the MTL uses the coronal plane or even oblique coronal plane perpendicular to the long axis of the hippocampus; the slab is typically 2 to 3 mm thick to improve the signal-to-noise ratio (SNR), but generally, a high in-plane resolution is used to maximize differences in the microanatomy. However, for diffusion EPI, the typical arrangement of coils in a multichannel receive array does not facilitate parallel acceleration in the coronal plane with the phase-encode direction superoinferiorly and requires the phase-encode direction to be along the left-right axis (acceleration factor 2; Fig. 3). Because EPI artifacts are severe along the lower bandwidth phase-encode axis, this results in asymmetric left-right distortion with a coronal plane acquisition using parallel imaging. With EPI in any orientation, the pattern of distortion will change depending on how the phase encoding axis is traversed; this is particularly difficult in the coronal plane (Figs. 4A, B).[53] Such asymmetries could surely confound quantitative analyses of connectivity. Distortion correction methods (Fig. 4C) can, to some extent, compensate for this but are neither widely available nor tested and may induce a degree of blurring. Finally, there is variable pneumatization of the adjacent petrous apices that causes a significant and possibly asymmetric degree of susceptibility-based distortion of the temporal lobes (Fig. 5B), which will be asymmetric in any coronal plane acquisition regardless of the phase-encode axis chosen.

The axial plane alleviates some of these asymmetries because, with typical coil arrangements, the phase-encode axis can be anteroposterior, preserving left-right symmetry while still allowing for parallel imaging (Fig. 6). The typical slice thickness of 2 to 2.2 mm is adequate for discerning the hippocampus from the adjacent substructures but is insufficient to visualize the intrahippocampal microstructure. Making slices thinner and voxels isotropic will quickly deplete the SNR to the point that noise dominates the results. For these reasons, the selection of slice thickness in the literature has varied from 2 to 5 mm (more often the latter), with the in-plane resolution varying from 1.8 to 3 mm. Anisotropic voxels that are small along 2 but not all 3 axes will preserve SNR, but this will result in bias in tractography and is generally avoided.[51]

The coil arrangement poses a particular challenge. Newer multichannel receiver arrays have the best SNR at the cortical surface. Volume coils have their best SNR at the center of the brain. The hippocampi are approximately halfway between the cortex and center of the brain, making any particular coil arrangement difficult to optimize.

TABLE 1. Diffusion Methods and Results Across Studies

Study	Subjects: AD/MCI/NC	Field Strength	Voxel Size	*B*	TE	Diffusion Directions—No. B_0 images, NEX	Parallel Imaging	Eddy Current Compensation or Correction	Motion Correction	*B* Matrix Correction	Other	Analysis	Significant Results
Fellgiebel et al[40]	19/14/10	1.5	1.8 × 1.8 × 5	900	100	6/1/1	N	N	N	N		ROI: FA/MD	L HC MD: AD>MCI>NC L HC FA: NC > MCI = AD
Müller et al[39]	0/18/18	1.5	1.8 × 1.8 × 5.0	900	100	6/1/1	N	N	N	N		ROI: FA/MD	B HC MD: MCI > NC B HC FA: NC > MCI
Rose et al[38]	0/17/17	1.5	1.8 × 1.8 × 2.8	1100	106	44/16/1	N	N	N	N		VBA: FA/MD	B ERC MD: MCI > NC B limbic FA: MCI < NC
Kalus et al[46]	10/10/10	1.5	3.3 × 2.5 × 2.5	1200	87	6/1/1	N	Dual echo	Y	—*		ROI: intervoxel coherence	B HC, ERC, and PPZ intervoxel coherence: NC > MCI > NC
Zhang et al[37]	17/17/18	1.5	2.3 × 2.3 × 5.0	1000	100	6/1/1	N	Dual echo	N	N	FLAIR	ROI: FA/MD	B HC MD: AD>NC (MCI NS) B HC FA: NC > MCI = AD
Salat et al[36]	74/0/54	1.5	2.0 × 2.0 × 2.0	700	89	60/10/1	N	Dual echo	FLIRT	—†		TBSS FA/MD, FA along PHG track	B MTL FA: NC > AD B MTL MD: AD > NC B PHG Tract Based FA: NC > AD
Mielke et al[47]	25/25/25	3.0	2.2 × 2.2 × 2.2	700	80	32/5/2	SENSE 2.5	AIR	AIR	N	B33 instead of B_0	ROI:FA	Fornix FA: NC = MCI > AD NS MTL differences between AD, MCI, and NC
Rogalski et al[41]	0/14/14	1.5	2.0 × 2.0 × 3.0	800	97	24/1/6	N	Rohde	Rohde	Y		ROI: FA/MD, FA/MD along PHG track	B PHG FA: NS difference B PHG MD: MCI > NC B PHG tract-based FA: NS B PHG tract-based MD: MCI > NC
Choo et al[42]	19/19/18	3.0	1.8 × 1.8 × 3.5	1000	77	25/1/1	N	Dual Echo	N	N		ROI: FA/MD	L PHG FA: NC > AD = MCI R PHG FA: NC > AD (MCI NS) B PHG MD: NS
Kantarci et al[33]	30/0/60 + 30 LBD	3T	3 × 3 × 3.3	1000	60	21/1/1	ASSET 2	AIR	AIR	N	FLAIR	VBA on MD (ROI based FA did not include the MTL)	B HC/PHG MD: AD > NC
Hong et al[35]	15/0/15 + 13 NPH	1.5	2.0 × 2.0 × 4.0	1000	83	25/1/1	N	N	N	N		ROI: FA/MD	B HC MD: AD > NC B HC FA: NC > AD
Yakushev et al[43]	20/0/0	1.5	1.8 × 1.8 × 3.0	1000	105	6/1/6	GRAPPA	N	Manual exclusion of motion-laden scans	N	FDG-PET also obtained	ROI: MD	L HC MD correlates inversely with FDG-PET and delayed verbal recall

A dash (–) indicates the information is not supplied in the article. NEX was assumed to be 1 if it was not listed. Similarly, the number of $b = 0$ images was also assumed to be 1 if not listed.

*A method of diffusion orientation compensation is cited in the eddy correction methods, but this method applies to rotating the tensor not rotating the raw diffusion images.[48]

†FSL can perform *B* matrix compensation after motion correction, but this article did not cite use of this compensation.

AIR indicates automated image registration[49]; HC, hippocampus; LBD, Lewy body dementia; NC, normal control; NPH, normal pressure hydrocephalus; NS, not significant; PPZ, perforant pathway zone; Rohde, Rohde et al[50]; SENSE, sensitivity encoding; TBSS, Tract-Based Spatial Statistics; VBA, voxel-based analysis.

FDG indicates fluorodeoxyglucose.

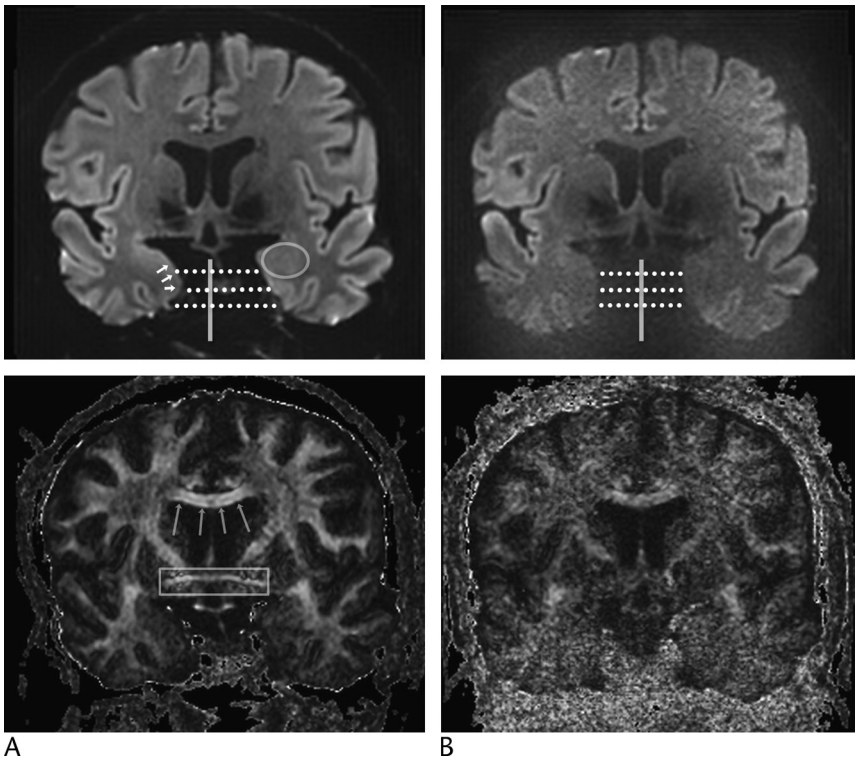

FIGURE 3. Coronal 3-mm-thick 1.2-mm in-plane diffusion-weighted EPI image at the anterior level of the anterior MTL. A circle surrounds the left amygdala. Short arrows outline the approximate location of the right ERC. Long arrows define the corpus callosum, and a box surrounds the anterior commissure. A, Phase-encode left to right with diffusion-weighted image at the top and FA at the bottom. This demonstrates asymmetric distortion along the left-right axis. B, Phase-encode superoinferior demonstrates left-right symmetry, but severe noise because of inadequate coil separation to support parallel imaging along this axis.

With regard to acquisition method, many reported studies have been done at 1.5 T, which offers inferior SNR to 3.0 T, although the newer studies are more often at 3.0 T. The SNR available even at 3.0 T creates a limit on the resolution that can be achieved in clinical scanning times. Going to 7.0 T has theoretical promise, but the tissue T2 and even more so the tissue T2* shorten as field strength increases, reducing the gain in SNR. In addition, B_1 inhomogeneity often results in asymmetric signal intensity within the temporal lobes. Methods are underway to improve visualization with 7 T.[54]

High-order shimming is known to improve B_0 homogeneity in the temporal lobes with echo-planar imaging and is available on clinical scanners.[55] The studies reported here did not describe the use of this procedure.

Microstructural interrogation requires extremely high-fidelity input imaging, and the typical diffusion-weighted imaging artifacts constitute a significant impediment. The addition of diffusion gradients results in eddy current artifacts as well as longer echo times with resulting low SNR. Compensating for eddy currents with a twice-refocused diffusion preparation scheme[56] results in an increase in echo time that further lowers the SNR; yet, adequate eddy current compensation is essential (Fig. 7). An alternative to twice-refocusing is the postprocessing technique.[50,57,58] However, only half of the studies reviewed here attempt to compensate for eddy currents using either of these correction approaches.

Patient motion is an additional factor that reduces data quality. Although approximately half of the studies reviewed here address issues in motion, only one study corrects for motion while adjusting the *b*-matrix, something that is known to improve accuracy and consistency.[52] Despite these attempts at motion correction, the registration of all diffusion time points

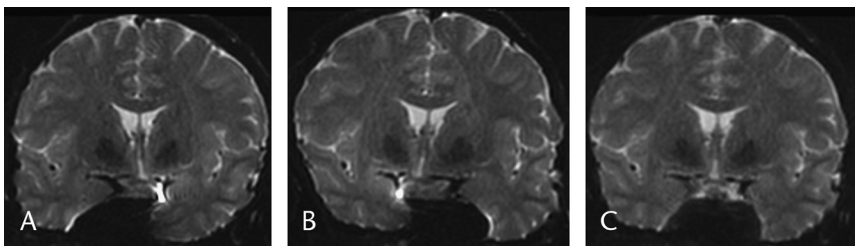

FIGURE 4. Coronal image of phase-encode traversal in one direction (A) and phase-encode traversal in the opposite direction (B). After correction (C), distortion is significantly reduced at the cost of minor blurring.

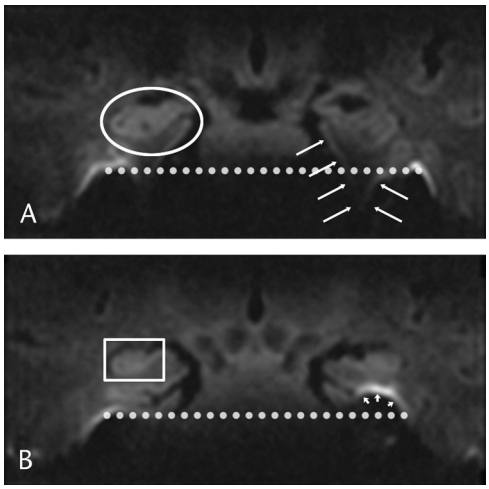

FIGURE 5. Zoom-EPI direct coronal acquisition. A, Anterior section. The right hippocampal head is circled. The left parahippocampal gyrus is outlined by arrows. Note distortion is present with inferior pointing of both parahippocampal gyri, but it is left-right symmetric (note the dotted horizontal line). B, Posterior section. The right hippocampal body is within the square. Because of differential pneumatization of the petrous apices, distortion is asymmetrically worse on the left parahippocampal gyrus (arrowheads) compared with the right, although the phase-encode axis is superoinferior.

with the $B = 0$ images is difficult to obtain on the fine scale required for the determination of microstructure.

Crossing fibers present an additional severe challenge for two reasons. First, the perforant pathway neurons cross a major white matter pathway, the cingulum bundle, which lies within the parahippocampal gyrus. Second, the perforant path crosses the subiculum to reach the dentate gyrus and remainder of the hippocampus; the gray matter of the subiculum may restrict diffusion because of its own internal structure, further confounding the analysis. Several methods exist to address crossing fibers,[59–65] but these generally require high b values, which starve the SNR (Fig. 8), and a large number of diffusion directions, which results in prohibitively long imaging times. To combat this SNR loss, larger voxel sizes are typically used, which again will be inadequate for microanatomy.

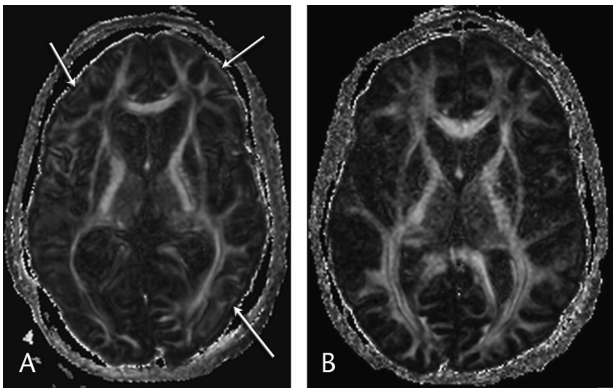

FIGURE 7. A, Single-refocused spin echo has better SNR but artificial FA at the cortices and edges of the image (arrows). B, Twice-refocused spin echo (on a different subject) has less SNR but less cortical FA artifact. Acquisitions are matched for imaging time.

It is clear that the interplay of a wide variety of imaging parameters can have a significant effect on the SNR, resolution, distortion, and others. The need to trade off between these measures of image quality explains the great variance in the parameters selected in the literature. B values range from 700 to 1200. The number of diffusion directions was most often 6, which is suboptimal for the measurement of FA and mean diffusivity

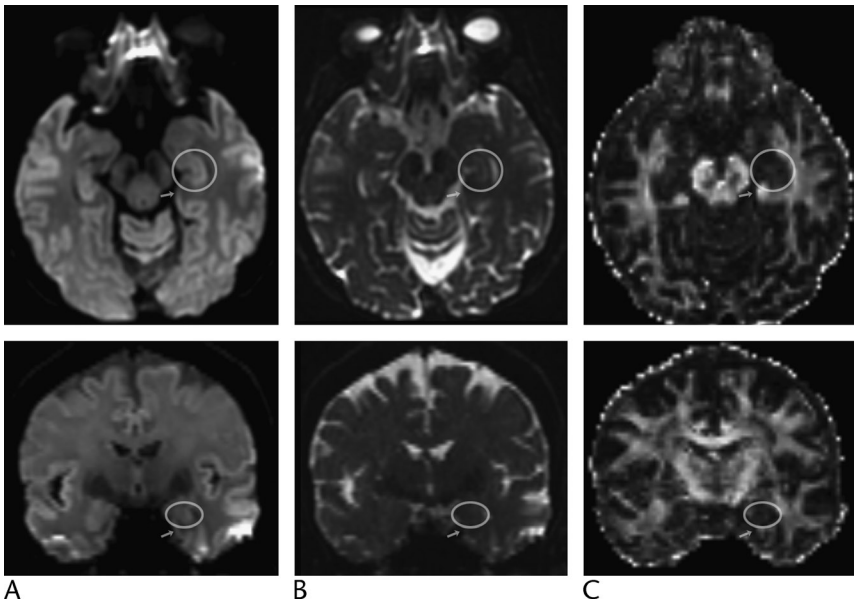

FIGURE 6. Top row: axial isotropic diffusion weighted EPI image (A), T2-weighted EPI (B), and FA map (C) at 3T with the phase-encode axis A-P and a 2mm isotropic acquisition. The left hippocampal head and amygdala are outlined by the circle, and an arrow points to the left parahippocampal gyrus (anterior parahippocampal gyrus on the coronal images, mid parahippocampal gyrus in the axial plane). These images demonstrate symmetric left-right distortion. Coronal reformats (bottom row) have inferior definition of medial temporal microstructure compared with anisotropic coronal acquisitions (Figs. 3A, 5, and 8) but demonstrate relatively symmetric distortion.

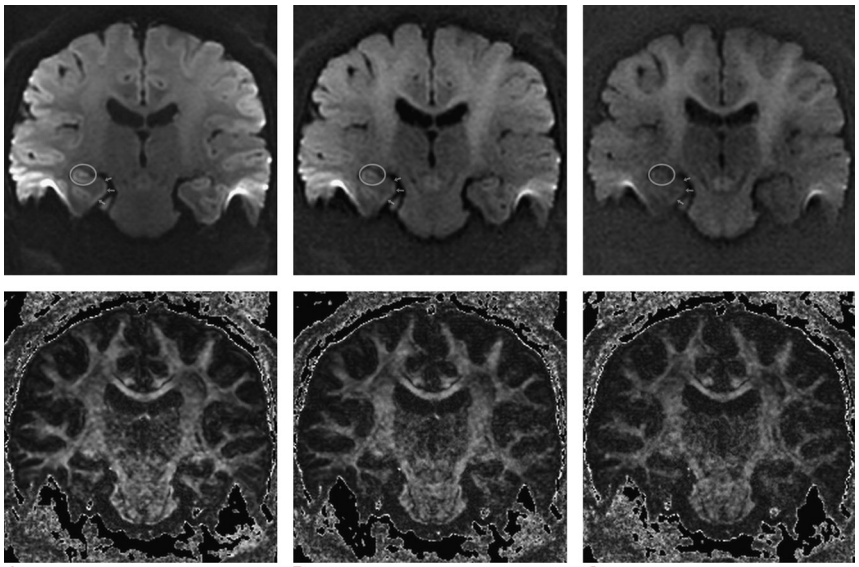

FIGURE 8. Coronal diffusion-weighted images (top) and FA maps for b = 1000 (A), b = 2000 (B), and b = 3000 (C). The right hippocampal body is encircled, and arrows outline the right parahippocampal gyrus. SNR progressively declines as the b value increases.

(MD),[66] but in one study, 60 directions were acquired. All acquisitions were in the axial plane, but some were oblique to the AC-PC line. Two studies use fluid attenuation inversion recovery (FLAIR) for CSF suppression, and one study replaces a b = 0-s/mm^2 image for a b = 33-s/mm^2 image without going into further details. Unfortunately, no single study uses parallel imaging, eddy current compensation, motion correction, and b matrix adjustment all together—all of which are validated to improve image quality.

Processing Issues

Diffusion image processing is hampered by numerous sources of rampant variability, including region of interest (ROI) selection and methodological differences in generating and quantifying tracts.

Region of interest selection dominates the methods of quantitative DTI processing, but the exact method of defining and even naming the ROI varies from study to study, although the studies generally use methods to ensure internal consistency. Region-of-interest analyses are best when there is extensive detail with regard to the segmentation criteria.[41] Interrater reliability measurements provide for internal consistency.[40] Unfortunately, all of the listed studies used very different segmentation procedures and criteria. In addition, if the segmentation procedure is not done on the b = 0 image, which is often the case, then the registration between the diffusion image and the structural image needs to be exact, and this requires at least a 9-parameter affine model to coregister the two. Ideally, segmentation should be performed or verified on the b = 0 image for each subject. In addition, there are relatively standardized references for determining the subregions of the MTL,[10] which can be the source of seed points for tractography.

Several studies go as far to distinguish hippocampal from parahippocampal ROIs, but with a slice thickness of 5 mm, the entire hippocampus fills a 5-mm voxel, and such distinction should be taken with caution.[37,39,40] A few studies use the term *entorhinal cortex*,[38,46] but a measurement of cortical FA unbiased by adjacent white matter is well beyond the resolution of any of the cited studies. Similarly, the fornix is 2 to 4 mm in cross section and would likely be subject to significant partial voluming effects.[47] These effects could statistically interact with patient category if there is generalized volume loss, which is the case in AD, even with FLAIR technique, which does not always result in complete CSF suppression. Two studies used voxel-based analyses[33,38]; this should be more objective and reproducible but would be more difficult to translate to clinical utility and would assume accurate registration, which is often difficult to quantify. Two studies performed tractography on the cingulum bundle within the parahippocampal gyrus and then measured FA and/or MD along the track.[36,41] This is an interesting form of analysis that isolates the track of interest, although its utility is complicated by crossing fibers in the same voxel that will contribute to the measured FA or MD.

Interpretation Challenges

When the bilateral hippocampi and parahippocampal structures are taken together as the MTL, most studies reported a significant difference in the MTL between AD and normal controls. This interpretation is complicated by the fact that some studies interpreted the hemispheres separately and others combined. Two studies reported significant results only for the left MTL. In most studies, results were significant for both FA and MD. However, in one study, results were significant for FA but not for MD,[42] and in another study, vice versa.[41] The reason for this is unknown. One of the listed studies revealed no MTL difference except for in the fornix.[47] This is for unclear reasons, and perhaps the somewhat low b value of 700 s/mm^2 coupled with a b = 33-s/mm^2 image rather than a b = 0-s/mm^2 image may be a factor. Alternatively, this study only evaluated MD, and perhaps a measurement of FA would have proven significant.

NON-AD MTL DIFFUSION STUDIES

In Vivo

An alternative acquisition scheme called Zoom-EPI has been applied in epilepsy to investigate the MTL.[67] Tilting the 180-degree-refocusing pulse results in a reduced field of view along 1 axis because it only partially intersects the 90-degree excitation slice. By choosing this axis as the phase-encode axis,

the number of phase-encode lines can be reduced, shortening the EPI readout, resulting in reduced distortions. The TE also shortens, offering a SNR gain, but this is offset by a SNR penalty from encoding fewer lines of *k*-space. In the coronal plane, this can be used to achieve high in-plane resolution, and distortion will be left-right symmetric with the phase-encode axis superoinferiorly. In this 1.5-T study, voxel size was 1.4 × 1.4 × 5 mm, facilitating detailed visualization of MTL anatomy, although a 10-mm slice gap required an interleaved acquisition. A Zoom-EPI image from our own implementation of the imaging sequence is demonstrated in Figure 5A. As is apparent, distortion is symmetric but still significant. Parallel imaging within slice cannot be added because typical head coil sensitivities will not be orthogonal enough along the shortened superoinferior phase-encode axis. Other inherent limitations to the Zoom technique include slice thickness, such that it may be difficult to extend the technique to isotropic voxels because the oblique pulse will interact with adjacent slices, as well as SNR reduction at the edges of the reduced field of view (because of the reduced effective slice thickness in these regions).

Another example of coronal plane DTI is a recent novel study examining the difference between younger and older individuals.[68] Here, the voxel size was 0.66 × 0.66 × 4 mm, with very high in-plane resolution. However, the voxels are anisotropic by a factor of 6, which could result in significant bias in tractography. The investigators thus chose an anatomy-driven definition of the perforant pathway and took the dot product of the expected pathway with the diffusion tensor, showing subtle differences between younger and older individuals. The study did use parallel imaging but did not specify the phase-encode axis. Likely, the phase-encode axis was left-right given the 8-channel head coil, and asymmetric distortion was necessarily present. This asymmetric distortion is an additional source of variance that can reduce sensitivity to significant findings in AD, especially because the diffusion literature suggests a slight increased importance of the left MTL. In other disease entities such as MTL sclerosis where left-right differences are key, this asymmetric distortion could be catastrophic for lesion detectability. The study used FMRIB software library/FLIRT for motion correction and eddy current compensation without description of *b*-matrix correction. The number of diffusion directions was 32 with a *b* value of 1200, and the NEX was very high at 12. This study is the first of its kind to push resolution with the aim of perforant pathway imaging, but SNR is admittedly low given the resolution.

Finally, a recent investigation using diffusion spectrum imaging is of interest, and the first of its kind with regard to the MTL. Six volunteers were scanned with 2.2 × 2.2 × 3.0-mm resolution, GRAPPA 2, $b = 8000$ (presumably with the use of insert gradients, although this was not described), 258 directions, one $b = 0$ image. Diffusion spectrum processing was performed, and their figures demonstrate reconstruction of the hippocampal-fornix output path to the mammillary bodies, as well as the parahippocampal cingulum bundle. Although interesting, tractography of the fornix can be accomplished with conventional tractography and quicker data acquisitions on conventional scanners[69] (Fig. 9). Crossing fiber resolved methods such as this will surely be a subject of future studies.

Ex Vivo

A 7-T study on hippocampal diffusion demonstrated variations in anisotropy and orientation throughout the hippocampal subfields.[72] Another study by the same author demonstrated further details in the rat hippocampus including the rat perforant pathway.[73]

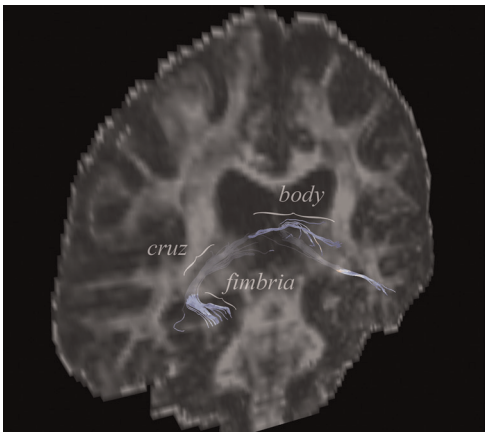

FIGURE 9. Tractography of the fornix. A whole brain b_{2000} data set at 3.0 T with 2-mm isotropic acquisition and 40 directions, processed with conventional DTI analysis using Camino, displayed with ParaView. Regions of interest were selected along the fornix with a waypoint in the fimbria of the fornix along the superior hippocampal body. An exclusion ROI was selected in the anterior hippocampal head. The fimbria, cruz, and body of the right fornix are labeled.[70,71] Figure 9 can be viewed online in color at www.topicsinmri.com.

A very impressive detailed tractography analysis of the MTL has recently been published.[74] At 4.7 T, specimens were imaged for 40 hours to achieve 200-μm isotropic data at a *b* value of 4000 with 20 directions at a TE of 28 using a 3D sequence. Tractography was performed deterministically with DTI Studio (https://www.mristudio.org) and probabilistically with eddy current correction using FSL's diffusion toolbox. Using either method, tracts were observed extending from the ERC to the subiculum and then from the subiculum to the CA fields and dentate gyrus. The subiculum was effectively a waypoint: all tractography stopped at this waypoint, and neither algorithm would trace directly from the ERC to the CA fields/dentate gyrus. This landmark study is the first of its kind to demonstrate known pathways on a microscopic level.

FUTURE DIRECTIONS

Performing high-quality DTI in an elderly patient population presents a technical challenge, and all of the articles cited in this study are of merit. Several points are obvious from this article to direct future endeavors. First, there is marked inconsistency in the literature with regard to MR methodology. None of the in vivo study examined in this article described use of parallel imaging, eddy current compensation, motion correction, and *b* matrix correction simultaneously. These are all tools available on all scanning platforms and with free software, so all future studies should use these methods.

A second point is regarding resolution. The resolution of a study needs to support the claims. Microstructure requires small pixels, volumetrically. Furthermore, all of the tractography programs have been developed with isotropic imaging to avoid directional bias. To advance the field, future work needs to pursue high-resolution isotropic imaging with low distortion. None of the listed studies offered a measurement of the SNR of their images. Although it is difficult to measure the SNR of diffusion-weighted images, one can easily measure the SNR of the $b = 0$ image with several repetitions; this only adds 1 minute at most to a sequence. Reporting this number will enable the scientific community to understand another source of variance.

Some newer methods of diffusion-weighted acquisition may provide a better balance of SNR and voxel size such as 3D balanced steady-state free precession imaging.[75] It is unclear if methods relying on the orientation of white matter with respect to the main magnetic field will prove to be applicable.[76–78]

Diffusion tensor imaging on specimens will help validate claims made by tractography, especially with the advance of methods that resolve crossing fibers. However, one needs to be cognizant of the limitations associated with fixed brains (eg, biological decay, volume change, significantly higher *b* value required, diffusion in blood vessels that contain flowing blood in vivo but ex vivo may have measurable diffusion characteristics, and larger susceptibility artifacts). Polarized light microscopy may help verify the results of tractography.[79]

IMPACT FOR CLINICAL AND RESEARCH DIFFUSION STUDIES OF THE MTL

This article suggests that future research studies and clinical work of the MTL, including AD and epilepsy, should adhere to the following guidelines.

Acquisition:

- 3 T imaging is preferable over 1.5 T
- Axial plane imaging with 2.0-mm isotropic voxels with the phase-encode axis anterior-posterior
  - To minimize partial voluming and keep distortions left-right symmetric
  - Coronal plane imaging can be pursued with anisotropic voxels, but caution should be exercised regarding distortions and bias in tractography
- High-order shimming to include at least second-order terms
  - To reduce B_0 inhomogeneity and associated image distortion
- Eddy current compensation either with twice-refocused diffusion preparation (dual spin echo) and/or correction using postprocessing
  - To reduce eddy current artifacts
- Motion correction and *b* matrix correction
  - Reduce the effect of motion and secondary effects of rotation on the direction of the encoding gradients. This may not necessarily be readily available clinically, but perhaps vendors will develop such tools
  - Visually examine (or use software) to exclude slices with severe signal dropouts because of patient motion or brain pulsation—peripheral gating can mitigate image quality but prolongs scan time, which is prohibitive in AD patients
- At least 30 diffusion directions for DTI[66,80]
- SNR measurement
  - Will facilitate standardization and the interpretation of differences among research studies

Processing:

- Segmentation of MTL structures
  - Either performed on or coregistered to the $b = 0$ images to ensure no misalignment
- Subregion analysis
  - Should refer to standard atlases[10]
- Measurement of both FA and MD

REFERENCES

1. Lewis FT. The significance of the term *hippocampus*. *J Comp Neurol*. 1923;35:213–230.
2. Walther C. Hippocampal terminology: concepts, misconceptions, origins. *Endeavour*. 2002;26:41–44.
3. Papez JW. A proposed mechanism of emotion. *Arch Neurol Psychiatry*. 1937;38:725–733.
4. Scoville WB, Milner B. Loss of recent memory after bilateral hippocampal lesions. *J Neurol Neurosurg Psychiatry*. 1957;20:11–21.
5. Milner B, Corkin S, Teuber HL. Further analysis of the hippocampal amnesic syndrome: 14-year follow-up study of H.M. *Neuropsychologia*. 1968;6:215–234.
6. Aggleton JP, Brown MW. Episodic memory, amnesia, and the hippocampal-anterior thalamic axis. *Behav Brain Sci*. 1999;22:425–444; discussion 444–489.
7. Zeineh MM, Engel SA, Thompson PM, et al. Unfolding the human hippocampus with high resolution structural and functional MRI. *Anat Rec*. 2001;265:111–120.
8. Nieuwenhuys R, Voogd J, Van Huijzen C, et al. *The Human Central Nervous System*. Berlin, Germany: Springer Verlag; 2008.
9. Duvernoy HM. *The Human Hippocampus: Functional Anatomy, Vascularization, and Serial Sections With MRI*. Berlin, Germany: Springer Verlag; 2005.
10. Insausti R, Amaral DG. Hippocampal formation. In: Paxinos G, Mai JK, eds. *The Human Nervous System*. 2nd ed. London, UK: Academic Press; 2004:871–914.
11. Suzuki WA, Amaral DG. Topographic organization of the reciprocal connections between the monkey entorhinal cortex and the perirhinal and parahippocampal cortices. *J Neurosci*. 1994;14(3 Pt 2):1856–1877.
12. Witter MP, Amaral DG. Entorhinal cortex of the monkey: V. Projections to the dentate gyrus, hippocampus, and subicular complex. *J Comp Neurol*. 1991;307:437–459.
13. Mufson EJ, Brady DR, Kordower JH. Tracing neuronal connections in postmortem human hippocampal complex with the carbocyanine dye DiI. *Neurobiol Aging*. 1990;11:649–653.
14. Hevner RF, Kinney HC. Reciprocal entorhinal-hippocampal connections established by human fetal midgestation. *J Comp Neurol*. 1996;372:384–394.
15. Braak H, Braak E. Neuropathological stageing of Alzheimer-related changes. *Acta Neuropathol*. 1991;82:239–259.
16. Mirra SS, Heyman A, McKeel D, et al. The Consortium to Establish a Registry for Alzheimer's Disease (CERAD). Part II. Standardization of the neuropathologic assessment of Alzheimer's disease. *Neurology*. 1991;41:479–486.
17. Trojanowski JQ, Lee VMY. The role of tau in Alzheimer's disease. *Med Clin North Am*. 2002;86:615–627.
18. Giannakopoulos P, Kövari E, Gold G, et al. Pathological substrates of cognitive decline in Alzheimer's disease. *Front Neurol Neurosci*. 2009;24:20–29.
19. Gómez-Isla T, Hollister R, West H, et al. Neuronal loss correlates with but exceeds neurofibrillary tangles in Alzheimer's disease. *Ann Neurol*. 1997;41:17–24.
20. Vemuri P, Wiste HJ, Weigand SD, et al. MRI and CSF biomarkers in normal, MCI, and AD subjects: predicting future clinical change. *Neurology*. 2009;73:294–301.
21. Lehéricy S, Marjanska M, Mesrob L, et al. Magnetic resonance imaging of Alzheimer's disease. *Eur Radiol*. 2007;17:347–362.
22. Bookheimer SY, Strojwas MH, Cohen MS, et al. Patterns of brain activation in people at risk for Alzheimer's disease. *N Engl J Med*. 2000;343:450–456.
23. Bookheimer S, Burggren A. APOE-4 genotype and neurophysiological vulnerability to Alzheimer's and cognitive aging. *Annu Rev Clin Psychol*. 2009;5:343–362.
24. Greicius MD, Srivastava G, Reiss AL, et al. Default-mode network activity distinguishes Alzheimer's disease from healthy aging: evidence from functional MRI. *Proc Natl Acad Sci U S A*. 2004;101:4637–4642.

25. Hess CP. Update on diffusion tensor imaging in Alzheimer's disease. *Magn Reson Imaging Clin N Am*. 2009;17:215–224.
26. Jack CR Jr, Knopman DS, Jagust WJ, et al. Hypothetical model of dynamic biomarkers of the Alzheimer's pathological cascade. *Lancet Neurol*. 2010;9:119–128.
27. Klunk WE, Engler H, Nordberg A, et al. Imaging brain amyloid in Alzheimer's disease with Pittsburgh compound-B. *Ann Neurol*. 2004;55:306–319.
28. Bacskai BJ, Frosch MP, Freeman SH, et al. Molecular imaging with Pittsburgh compound B confirmed at autopsy: a case report. *Arch Neurol*. 2007;64:431–434.
29. Gómez-Isla T, Price JL, McKeel DW Jr, et al. Profound loss of layer II entorhinal cortex neurons occurs in very mild Alzheimer's disease. *J Neurosci*. 1996;16:4491–4500.
30. Hyman BT, Van Hoesen GW, Damasio AR, et al. Alzheimer's disease: cell-specific pathology isolates the hippocampal formation. *Science*. 1984;225:1168–1170.
31. Van Hoesen GW, Hyman BT, Damasio AR. Entorhinal cortex pathology in Alzheimer's disease. *Hippocampus*. 1991;1:1–8.
32. Beaulieu C. The basis of anisotropic water diffusion in the nervous system—a technical review. *NMR Biomed*. 2002;15:435–455.
33. Kantarci K, Avula R, Senjem ML, et al. Dementia with Lewy bodies and Alzheimer disease: neurodegenerative patterns characterized by DTI. *Neurology*. 2010;74:1814–1821.
34. Sexton CE, Kalu UG, Filippini N, et al. A meta-analysis of diffusion tensor imaging in mild cognitive impairment and Alzheimer's disease. *Neurobiol Aging*. 2010;32:2322.e5–e18.
35. Hong YJ, Yoon B, Shim YS, et al. Differences in microstructural alterations of the hippocampus in Alzheimer disease and idiopathic normal pressure hydrocephalus: a diffusion tensor imaging study. *AJNR Am J Neuroradiol*. 2010;31:1867–1872.
36. Salat DH, Tuch DS, van der Kouwe AJW, et al. White matter pathology isolates the hippocampal formation in Alzheimer's disease. *Neurobiol Aging*. 2010;31:244–256.
37. Zhang Y, Schuff N, Jahng G, et al. Diffusion tensor imaging of cingulum fibers in mild cognitive impairment and Alzheimer disease. *Neurology*. 2007;68:13–19.
38. Rose SE, McMahon KL, Janke AL, et al. Diffusion indices on magnetic resonance imaging and neuropsychological performance in amnestic mild cognitive impairment. *J Neurol Neurosurg Psychiatry*. 2006;77:1122–1128.
39. Müller MJ, Greverus D, Dellani PR, et al. Functional implications of hippocampal volume and diffusivity in mild cognitive impairment. *Neuroimage*. 2005;28:1033–1042.
40. Fellgiebel A, Wille P, Müller MJ, et al. Ultrastructural hippocampal and white matter alterations in mild cognitive impairment: a diffusion tensor imaging study. *Dement Geriatr Cogn Disord*. 2004;18:101–108.
41. Rogalski EJ, Murphy CM, deToledo-Morrell L, et al. Changes in parahippocampal white matter integrity in amnestic mild cognitive impairment: a diffusion tensor imaging study. *Behav Neurol*. 2009;21:51–61.
42. Choo IH, Lee DY, Oh JS, et al. Posterior cingulate cortex atrophy and regional cingulum disruption in mild cognitive impairment and Alzheimer's disease. *Neurobiol Aging*. 2010;31:772–779.
43. Yakushev I, Gerhard A, Müller MJ, et al. Relationships between hippocampal microstructure, metabolism, and function in early Alzheimer's disease. *Brain Struct Funct*. 2011;216:219–226.
44. Chua TC, Wen W, Slavin MJ, et al. Diffusion tensor imaging in mild cognitive impairment and Alzheimer's disease: a review. *Curr Opin Neurol*. 2008;21:83–92.
45. Stebbins GT, Murphy CM. Diffusion tensor imaging in Alzheimer's disease and mild cognitive impairment. *Behav Neurol*. 2009;21:39–49.
46. Kalus P, Slotboom J, Gallinat J, et al. Examining the gateway to the limbic system with diffusion tensor imaging: the perforant pathway in dementia. *Neuroimage*. 2006;30:713–720.
47. Mielke MM, Kozauer NA, Chan KCG, et al. Regionally-specific diffusion tensor imaging in mild cognitive impairment and Alzheimer's disease. *Neuroimage*. 2009;46:47–55.
48. Alexander DC, Pierpaoli C, Basser PJ, et al. Spatial transformations of diffusion tensor magnetic resonance images. *IEEE Trans Med Imaging*. 2001;20:1131–1139.
49. Woods RP, Grafton ST, Holmes CJ, et al. Automated image registration: I. General methods and intrasubject, intramodality validation. *J Comput Assist Tomogr*. 1998;22:139–152.
50. Rohde GK, Barnett AS, Basser PJ, et al. Comprehensive approach for correction of motion and distortion in diffusion-weighted MRI. *Magn Reson Med*. 2004;51:103–114.
51. Jones DK, Leemans A. Diffusion tensor imaging. *Methods Mol Biol*. 2011;711:127–144.
52. Jones DK, Cercignani M. Twenty-five pitfalls in the analysis of diffusion MRI data. *NMR Biomed*. 2010;23:803–820.
53. Embleton KV, Haroon HA, Morris DM, et al. Distortion correction for diffusion-weighted MRI tractography and fMRI in the temporal lobes. *Hum Brain Mapp*. 2010;31:1570–1587.
54. von Morze C, Kelley DAC, Shepherd TM, et al. Reduced field-of-view diffusion-weighted imaging of the brain at 7 T. *Magn Reson Imaging*. 2010;28:1541–1545.
55. Kim D, Adalsteinsson E, Glover GH, et al. Regularized higher-order in vivo shimming. *Magn Reson Med*. 2002;48:715–722.
56. Reese TG, Heid O, Weisskoff RM, et al. Reduction of eddy-current–induced distortion in diffusion MRI using a twice-refocused spin echo. *Magn Reson Med*. 2003;49:177–182.
57. Andersson JLR, Skare S. A model-based method for retrospective correction of geometric distortions in diffusion-weighted EPI. *Neuroimage*. 2002;16:177–199.
58. Haselgrove JC, Moore JR. Correction for distortion of echo-planar images used to calculate the apparent diffusion coefficient. *Magn Reson Med*. 1996;36:960–964.
59. Frank LR. Anisotropy in high angular resolution diffusion-weighted MRI. *Magn Reson Med*. 2001;45:935–939.
60. Frank LR. Characterization of anisotropy in high angular resolution diffusion-weighted MRI. *Magn Reson Med*. 2002;47:1083–1099.
61. Wedeen VJ, Wang RP, Schmahmann JD, et al. Diffusion spectrum magnetic resonance imaging (DSI) tractography of crossing fibers. *Neuroimage*. 2008;41:1267–1277.
62. Wedeen VJ, Hagmann P, Tseng WI, et al. Mapping complex tissue architecture with diffusion spectrum magnetic resonance imaging. *Magn Reson Med*. 2005;54:1377–1386.
63. Tuch DS. Q-ball imaging. *Magn Reson Med*. 2004;52:1358–1372.
64. Tournier J, Yeh C, Calamante F, et al. Resolving crossing fibres using constrained spherical deconvolution: validation using diffusion-weighted imaging phantom data. *Neuroimage*. 2008;42:617–625.
65. Alexander DC. Maximum entropy spherical deconvolution for diffusion MRI. *Inf Process Med Imaging*. 2005;19:76–87.
66. Jones DK. The effect of gradient sampling schemes on measures derived from diffusion tensor MRI: a Monte Carlo study. *Magn Reson Med*. 2004;51:807–815.

67. Salmenpera TM, Simister RJ, Bartlett P, et al. High-resolution diffusion tensor imaging of the hippocampus in temporal lobe epilepsy. *Epilepsy Res*. 2006;71:102–106.
68. Yassa MA, Muftuler LT, Stark CEL. Ultrahigh-resolution microstructural diffusion tensor imaging reveals perforant path degradation in aged humans in vivo. *Proc Natl Acad Sci U S A*. 2010;107:12687–12691.
69. Concha L, Livy DJ, Beaulieu C, et al. In vivo diffusion tensor imaging and histopathology of the fimbria-fornix in temporal lobe epilepsy. *J Neurosci*. 2010;30:996–1002.
70. Cook P, Bai Y, Nedjati-Gilani S, et al. Camino: Open-source diffusion-MRI reconstruction and processing. In: *14th Scientific Meeting of the International Society for Magnetic Resonance in Medicine*. 2006;2759.
71. Basser PJ, Mattiello J, LeBihan D. Estimation of the effective self-diffusion tensor from the NMR spin echo. *J Magn Reson B*. 1994;103:247–254.
72. Shepherd TM, Ozarslan E, Yachnis AT, et al. Diffusion tensor microscopy indicates the cytoarchitectural basis for diffusion anisotropy in the human hippocampus. *AJNR Am J Neuroradiol*. 2007;28:958–964.
73. Shepherd TM, Ozarslan E, King MA, et al. Structural insights from high-resolution diffusion tensor imaging and tractography of the isolated rat hippocampus. *Neuroimage*. 2006;32:1499–1509.
74. Augustinack JC, Helmer K, Huber KE, et al. Direct visualization of the perforant pathway in the human brain with ex vivo diffusion tensor imaging. *Front Hum Neurosci*. 2010;4:42.
75. McNab JA, Miller KL. Steady-state diffusion-weighted imaging: theory, acquisition and analysis. *NMR Biomed*. 2010;23:781–793.
76. Liu C. Susceptibility tensor imaging. *Magn Reson Med*. 2010;63:1471–1477.
77. Miller KL, Smith SM, Jezzard P. Asymmetries of the balanced SSFP profile. Part II: White matter. *Magn Reson Med*. 2010;63:396–406.
78. Miller KL. Asymmetries of the balanced SSFP profile. Part I: Theory and observation. *Magn Reson Med*. 2010;63:385–395.
79. Axer M, Amunts K, Grässel D, et al. A novel approach to the human connectome: ultra-high resolution mapping of fiber tracts in the brain. *Neuroimage*. 2011;54:1091–1101.
80. Skare S, Hedehus M, Moseley ME, et al. Condition number as a measure of noise performance of diffusion tensor data acquisition schemes with MRI. *J Magn Reson*. 2000;147:340–352.